

Bipolar Resistive Switching Characteristics of Ex-situ Synthesized TiO₂-ZnO Nanocomposite

Rutuja U. Amate^{1,*}, Pritam J. Morankar¹, Navaj B. Mullani², Kishorkumar V. Khot¹,
Rajanish K. Kamat³, Tukaram D. Dongale^{1,†}, Deok-kee Kim^{4,‡}

¹ Computational Electronics and Nanoscience Research Laboratory, School of Nanoscience and Biotechnology,
Shivaji University, Kolhapur 416004, India

² Department of Materials Science & Chemical Engineering, Hanyang University, Ansan 15588, Korea

³ Department of Electronics, Shivaji University, Kolhapur 416004, India

⁴ Department of Electrical Engineering, Sejong University, 209, Neungdong-ro, Gwangjin-gu,
Seoul 05006, Republic of Korea

(Received 15 February 2020; revised manuscript received 15 April 2020; published online 25 April 2020)

In this present article, we have reported a simple and cost-effective ex-situ synthesis of TiO₂-ZnO (TZ) nanocomposite thin film by utilizing sol-gel, hydrothermal and solid-state reaction methods. The Ag/TZ/FTO nanocomposite device was developed and demonstrated the bipolar resistive switching (RS) characteristics for resistive memory applications. The result of XRD analysis confirms that the nanocomposite has mixed tetragonal and hexagonal crystal structures of TiO₂ and ZnO, respectively. The hysteresis loop is an essential criterion for recognizing memristive devices and similar characteristic was noticed for the developed nanocomposite device. Besides, basic memristive properties were calculated from the I-V data. The charge transportation of Ag/TZ/FTO nanocomposite device takes place because of Ohmic and space charge limited current. The collective effect of oxygen vacancies and Ag ions was a basis of RS effect in the Ag/TZ/FTO nanocomposite device.

Keywords: Memristive device, Nanocomposite, Resistive switching.

DOI: [10.21272/jnep.12\(2\).02025](https://doi.org/10.21272/jnep.12(2).02025)

PACS numbers: 78.67.Sc, 68.55. - a, 81.07. - b

1. INTRODUCTION

The memory devices are essential elements in the digital electronics which can store and retrieve the enormous amount of information and also plays a vital role in the big data innovation in recent years. Recently, memristive devices become an important topic of research and innovation owing to their passivity and memory property [1]. The memristive devices are work on the well-known resistive switching (RS) mechanism and store data in terms of the resistance state of the device. It is a physical phenomenon, in which the resistance of material changes due to the application of the electric field [2]. The recent studies suggested that RS based devices are promising next-generation memory devices and can replace flash memory in the near future [3]. In addition to this, the memristive and RS devices have significant applications in the field of biomedical, neural computing, nonlinear dynamics circuits and sensors [4-6].

Among them, the metal oxides are popular among the many research groups owing to its cost-effectiveness, fabrication friendliness, and tune ability of the material properties [8]. Currently, transition metal oxide-based nanocomposites are attracting much interest because of its outstanding chemical, optical and electronic properties [9]. The abundant oxygen vacancies in the TiO₂ makes it a promising oxide material for RS applications. These vacancies play an important role in the development and breakdown of conductive filament [10]. In addition to this, TiO₂ possesses excellent electrical and optical properties along with

the nonappearance of toxicity and good chemical stability. On the other hand, ZnO is a direct bandgap semiconductor with high electron mobility [11]. The TiO₂ and ZnO are well-known and promising materials to achieve better RS properties. In addition to this, a composite of TiO₂ and ZnO are non-toxic and can quickly fabricate with minimal efforts.

In this work, we have synthesized the TiO₂-ZnO (TZ) nanocomposite using the ex-situ method, which can be utilized as a switching layer for resistive memory application with Ag/TZ/FTO device configuration. The ex-situ synthesis of TZ nanocomposite was carried out by using a solid-state reaction approach at room temperature, followed by the deposition on FTO using the doctor blade method. The electrical measurements demonstrated that the Ag/TZ/FTO device has good RS properties.

2. EXPERIMENTAL

2.1 Materials

The zinc acetate ((CH₃COO)₂ZnO·2H₂O) was utilized to synthesis ZnO, whereas the titanium isopropoxide (TTIP, C₁₂H₂₈O₄Ti) was used to synthesis TiO₂. Ammonia (NH₃) and acetic acid (CH₃COOH), sodium dodecyl sulphate (SDS), were used as reagents to complete the metal oxide reaction. Ethyl-cellulose, lauric acid, terpineol and ethanol were used for the doctor blade deposition process.

* rutuja.nanotechnology@gmail.com

† tdd.snst@unishivaji.ac.in

‡ deokkeekim@sejong.ac.kr

2.2 Synthesis of ZnO Nanopowder

In the present case, the ZnO nanopowder was synthesized by hydrothermal route. Initially, 0.1 M of zinc acetate was dissolved in 500 ml of double distilled water under constant stirring. Then, NH_3 was included in the above solution, leading to form white precipitates in the reaction bath. As the drop wise additions of NH_3 continue, the white precipitates disappear and then the solution becomes colorless. Once a transparent and clear solution appeared, the solution was transferred into a beaker and covered with Al foil and then kept in an autoclave for 1hr at 90 °C to complete the reaction. After this, the product was collected and washed with ethanol. Finally, the product was centrifuged at 7000 rpm for 15 min and annealed at 350 °C for 2 h.

2.3 Synthesis of TiO_2 Nanopowder

The sol-gel method was adopted for the synthesis of TiO_2 nanopowder. Initially, 5 ml TTIP and 5 ml acetic acid were taken in a beaker (solution A). In another beaker, 0.4 wt. % SDS was and mixed in the 100 ml double distilled water (solution B). Both solutions were stirred continuously for 15 min. to make a homogeneous solution. Later, solution B was poured into solution A and stirred for 4 h at room temperature (pH ~ 10). The precipitated solution was collected by the decantation process and gel type of product was collected for the washing. The washing was done by using the solvents, ethanol: water (30:70) ratio to neutralize the product. The repeated (3 times) centrifugation was done at 7000 rpm for 10 min. The obtained product was dried in an oven at 60 °C and finally annealed at 450 °C for 2 h.

2.4 Synthesis of TZ Nanocomposite and Fabrication of the Device

The ex-situ TZ nanocomposite was synthesized by using a solid-state reaction method by employing TiO_2 and ZnO. Initially, the TiO_2 and ZnO took in the ratio of 80:20 and crushed very well for 3 h using mortar and pestle. The resulting powder was annealed in the furnace at 500 °C for 1 h. The simplified process of the doctor blade deposition method [12] for the build-out of TZ nanocomposite is shown in Fig. 1a. Firstly, 0.05 g of TZ nanocomposite powder was crushed for 15 min. by adding 0.05 g of lauric acid by using mortar and pestle. Furthermore, the alpha-terpineol binder was added during grinding. Upon the formation of viscous slurry, few drops of ethylene glycol were added and gently mixed for 10 min. In the second step, the nanocomposite paste was applied on the FTO substrate. The deposited paste was dried at 70 °C for 30 min and finally annealed at 120 °C for 10 min and 450 °C for 30 min. to expel the binder related species and impurities from the TZ in nanocomposite thin film. Finally, Ag was patterned on the active switching layer to frame the Ag/TZ/FTO thin-film device.

3. RESULTS AND DISCUSSION

The XRD spectra of TZ nanocomposite is shown in Fig. 1b. The phase identification and crystalline size of the metal oxide composite were determined by using the XRD spectra with CuK α wavelength ~ 1.54 Å (D2 phas-

er, Bruker). The sharp and intense XRD peaks of both oxides are clearly observed in the XRD pattern. The crystallinity of the material is identified with matching obtained data with the corresponding JCPDS card. The resulted XRD pattern of TiO_2 is well-matched with anatase phase and tetragonal crystal structure (JCPDS No. 01-078-2486). The major diffraction peaks of TiO_2 were observed at 25.30°, 37.86°, 48.04°, 53.97°, 75.14°, and 82.72° which are associated with the (101), (004), (200), (105), (215) and (224) crystal planes, respectively. In addition, the existence of other clear and sharp peaks at 31.72°, 34.40°, 36.21°, 56.51°, 62.80°, 67.85, and 69.08 correspond to (100), (002), (101), (110), (103), (112) and (201) crystal planes, respectively. The obtained peaks of ZnO were well indexed with JCPDS card No. 01-079-0206 confirming the presence of ZnO in the hexagonal wurtzite crystal structure. From XRD analysis, it was confirmed that the prepared metal oxide nanocomposite has tetragonal TiO_2 and hexagonal ZnO crystal structures. The crystallite size for TZ nanocomposite was found to be 7.20 nm, which demonstrates the prepared composite is in nanocrystalline nature [13]. The microstrain and dislocation density of the nanocomposite was $1.98 \cdot 10^{-3} \text{ lines}^{-2} \cdot \text{m}^{-4}$ and $19.28 \cdot 10^{-3} \text{ lines} \cdot \text{m}^{-2}$, respectively. The lower value of microstrain and dislocation density indicates that the very less amount of lattice distortions or imperfections were present in the prepared nanocomposite.

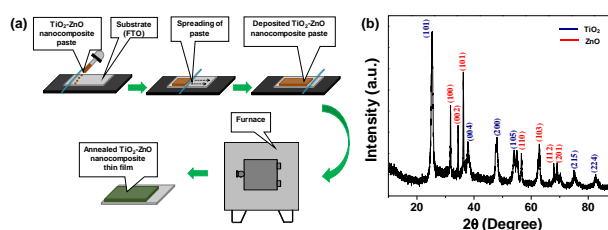


Fig. 1 – Schematic illustration of the doctor blade deposition process to develop the TZ nanocomposite thin film (a); XRD spectra of the TZ nanocomposite (b)

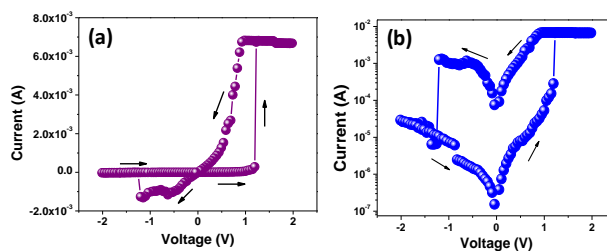


Fig. 2 – I - V characteristic of Ag/TZ/FTO device in linear (a) and semi log scale (b)

The RS properties of the prepared nanocomposite were determined by the memristor characterization system (ArC ONE). The pinched hysteresis loop was observed in the current-voltage (I - V) plane, be seen in Fig. 2. In the present case, the device switch to LRS from the HRS at +1.20 V (SET voltage) and again switch to HRS from LRS at -1.22 V (RESET voltage). The device shows the nearly symmetric switching voltages, however, asymmetric hysteresis loops were observed in the present case. The obtained hysteresis loop from the developed device confirms that the prepared nanocomposite device showing the bipolar RS property. The obtained bipolar

nature of the device is showing the selector device like characteristics. At a lower voltage region, a modest quantity of current was passed through the device and therefore showed the HRS. Afterward, the current increases at the SET voltage and the device switch to LRS. The rapid increase in current is related to the abrupt nature of the formation of conducting filament due to the oxygen vacancies and Ag ions. The calculated dislocation density and microstrain of the composite structure showing the little increase in the interstitial planes of both oxides. This helps to assist the effective generation and breakdown of conducting filament.

In order to study the memristive nature of the Ag/TZ/FTO device, different properties such as time-domain voltage, current, charge, and magnetic flux were drawn out from the $I-V$ data, as shown in Fig. 3. The device demonstrates a sudden change in the current by applying the staircase type (\sim triangular) input voltage, as shown in Fig. 3a. This kind of abrupt nature is useful for the resistive memory application. The usual symmetric time-domain flux characteristic was observed, as displayed in Fig. 3b. Consequently, asymmetric time-domain charge characteristic was found in the case of the nanocomposite device, as displayed in Fig. 3c. Interestingly, a developed nanocomposite device demonstrates two-valued charge-magnetic flux relation, as shown in Fig. 3d. The two-valued charge-magnetic flux nature suggested the dominance of the memristive property in the of the Ag/TZ/FTO device [14].

By plotting the $\log I-\log V$ characteristics and fitting the appropriate charge transport models to the HRS data, we can study the conduction mechanism of the device and one such results are shown in Fig. 4. For this, the slope values of the positive and negative biased low and high voltage regions were determined and summarized in Fig. 4a and Fig. 4b. The Ohmic model shows good fitting to positive and negative biased the low voltage region, as shown in Fig. 4c and Fig. 4d. In the case of positive and negative biased high voltage region, the Child's square law model is well fitted to experimental data, as shown in the Fig. 4e and Fig. 4f. For both bias regions (positive and negative), the rapid increment in the current was noticed – this kind of behavior pointing towards the SCLC conduction mechanism [15].

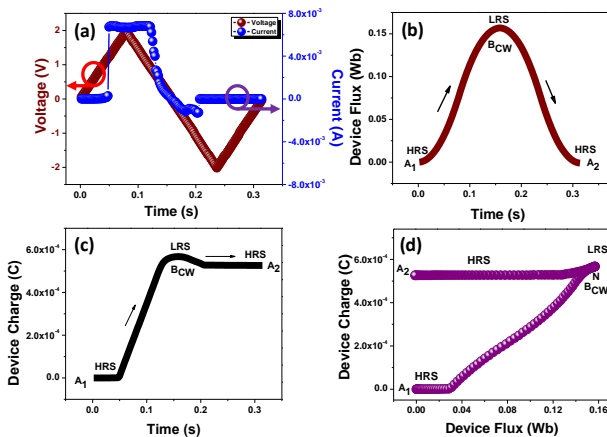


Fig. 3 – Time-domain input voltage and output current nature of the Ag/TZ/FTO device (a); time-domain flux (b), charge (c) and charge-flux (d) characteristics of Ag/TZ/FTO device

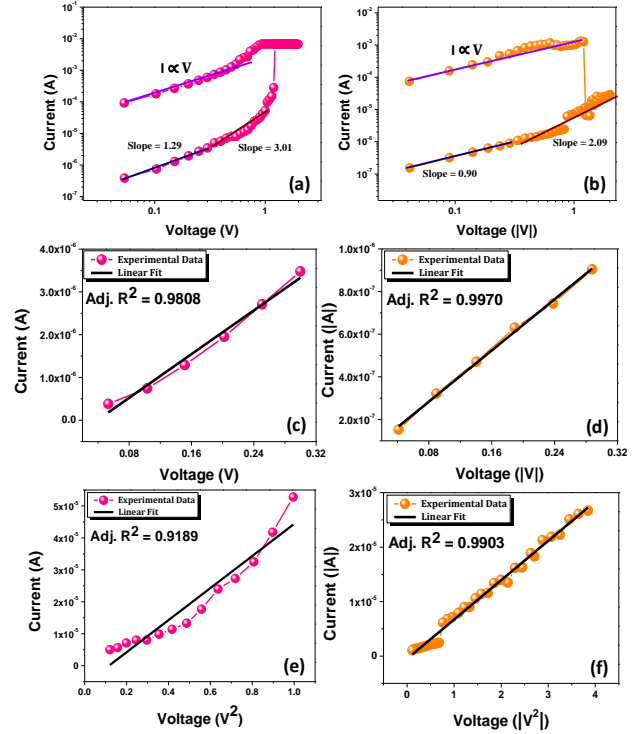


Fig. 4 – Double logarithmic $I-V$ characteristic of Ag/TZ/FTO thin film memristive device in the positive (a) and negative (b) bias regions. The Ohmic conduction mechanism fitting to the positive biased (c) and negative biased (d) low voltage regions. Child's square law fitting to the positive biased (e) and negative biased (f) high voltage regions

Based on the model fitting results, a filamentary RS mechanism is shown in Fig. 5. In the case of oxide memory devices, the RS behavior is generally depending on the ionic transportation of oxygen vacancies [10], whereas active top electrode (Ag or Cu) based devices work on the redox reaction of the top electrode [16]. In the present case, both types of mechanisms could be present because of the inherent availability of the oxygen vacancies in the TZ nanocomposite and utilization of Ag as a top electrode. When positive bias voltage was provided to the top electrode, the Ag gets oxidized into Ag^+ ions and drifted towards the bottom electrode, results in the building of the Ag-based filament. In addition to this, oxygen vacancies present in the active switching layer also drift towards the bottom electrode due to the applied bias to the top electrode. Given this, Ag and oxygen vacancies start to form a conductive filament and current of the device gradually increases. As the given voltage increases, the density of the filament increases and the device switch to the LRS. This completely developed conductive filament promotes to switch the device in ON (LRS) state. In the following stage, under the influence of negative bias voltage, the Ag is oxidized and oxygen vacancies are drift towards the top electrode. This results in the starting of the dissolution of the conductive filament. The conductive filament completely ruptures at the RESET voltage and the device switch to the OFF (HRS) state.

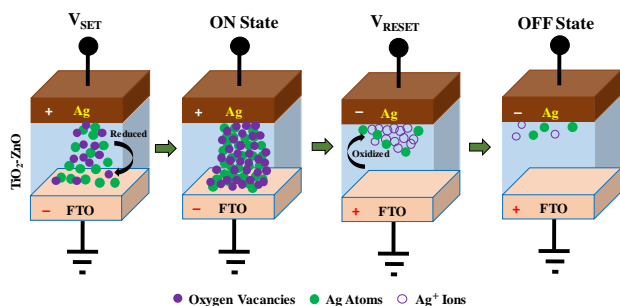


Fig. 5 – A possible bipolar RS mechanism of the Ag/TZ/FTO nanocomposite thin film memristive device

4. CONCLUSIONS

We have synthesized the TZ nanocomposite device using a solution-processable technique and demonstrated the bipolar RS properties. The XRD data confirm that the nanocomposite has mixed tetragonal and hexagonal crystal structures of TiO_2 and ZnO , respectively. The lower value of microstrain and dislocation

density indicates that the very less amount of lattice distortions or imperfections were present in the prepared nanocomposite. The device shows the nearly symmetric switching voltages; however, asymmetric hysteresis loops were observed in the present case. The two-valued charge-magnetic flux nature suggested the dominance of the memristive property in the of the Ag/TZ/FTO device. The SCLC conduction mechanism was dominated in the HRS whereas; LRS was due to the Ohmic conduction mechanism. The filamentary switching based on Ag and oxygen vacancies leads to the bipolar RS effect in Ag/TZ/FTO memristive device.

ACKNOWLEDGEMENTS

This study was supported by the Basic research program (2016R1D1A1B01009537) through the National Research Foundation (NRF) of Korea and by the MOTIE (Ministry of Trade, Industry and Energy (10080581) and KSRC (Korea Semiconductor Research Consortium) support program for the development of the future semiconductor device.

REFERENCES

1. C. Sung, H. Hwang, I.K. Yoo, *J. Appl. Phys.* **124**, 151903 (2018).
2. V.L. Patil, A.A. Patil, S.V. Patil, N.A. Khairnar, N.L. Tarwal, S.A. Vanalakar, R.N. Bulakhe, I. In, P.S. Patil, T.D. Dongale, *Mater. Sci. Semicond. Process.* **106**, 104769 (2020).
3. T.S. Bhat, A.S. Kalekar, D.S. Dalavi, C.C. Revadekar, A.C. Khot, T.D. Dongale, P.S. Patil, *J. Mater. Sci-Mater. Ele.* **30**, 17725 (2019).
4. Z.H. Tan, R. Yang, K. Terabe, X.B. Yin, X.D. Zhang, X. Guo, *Adv. Mater.* **28**, 377 (2016).
5. A.H. Edwards, H.J. Barnaby, K.A. Campbell, M.N. Kozicki, W. Liu, M.J. Marinella, *Proc. IEEE.* **103**, 1004 (2015).
6. A.V. Pawar, S.S. Kanapally, K.D. Kadam, S.L. Patil, V.S. Dongle, S.A. Jadhav, S. Kim, T.D. Dongale, *J. Mater. Sci-Mater. Ele.* **30**, 11383 (2019).
7. S.G. Kim, J.S. Han, H. Kim, S.Y. Kim, H.W. Jang, *Mater. Sci. Forum* **3**, 1800457 (2018).
8. S.S. More, P.A. Patil, K.D. Kadam, H.S. Patil, S.L. Patil, A.V. Pawar, S.S. Kanapally, D.V. Desai, S.M. Bodake, R.K. Kamat, S. Kim, *Results Phys.* **12**, 1946 (2019).
9. G. Korotcenkov, B.K. Cho, *Sensors and Actuators B: Chemical.* **244**, 182 (2017).
10. C. Ye, T. Deng, T. Zhang, L. Shen, P. He, W. Wei, H. Wang, *Semicond. Sci. Technol.* **31**, 105005 (2016).
11. C. Hu, Q. Wang, S. Bai, M. Xu, D. He, D. Lyu, J. Qi, *Appl. Phys. Lett.* **110**, 073501 (2017).
12. S. Patil, M. Chougale, T. Rane, S. Khot, A. Patil, O. Bagal, S. Jadhav, A. Sheikh, S. Kim, T. Dongale, *Electronics* **7**, 445 (2018).
13. N. Hellen, H. Park, K.N. Kim, *J. Korean Ceram. Soc.* **55**, 140 (2018).
14. L. Chua, *IEEE Trans. Circuits Syst.* **18**, 507 (1971).
15. T.D. Dongale, K.P. Patil, P.K. Gaikwad, R.K. Kamat, *Mater. Sci. Semicond. Process.* **38**, 228 (2015).
16. C.P. Hsiung, H.W. Liao, J.Y. Gan, T.B. Wu, J.C. Hwang, F. Chen, M.J. Tsai, *ACS Nano.* **4**, 5414 (2010).